Old Dominion University
ODU Digital Commons

Bioelectrics Publications   Frank Reidy Research Center for Bioelectrics

2012

Probing Nanoparticle Interactions in Cell Culture Media

Ahmet C. Sabuncu
Old Dominion University

Janna Grubbs
Old Dominion University

Shizhi Qian
Old Dominion University

Tarek M. Abdel-Fattah

Michael W. Stacey
Old Dominion University, mstacey@odu.edu

See next page for additional authors

Follow this and additional works at: https://digitalcommons.odu.edu/bioelectrics_pubs

Part of the Biomedical Engineering and Bioengineering Commons, Cell and Developmental Biology Commons, and the Nanotechnology Commons

Authors

Ahmet C. Sabuncu, Janna Grubbs, Shizhi Qian, Tarek M. Abdel-Fattah, Michael W. Stacey, and Ali Beskok

Probing nanoparticle interactions in cell culture media

Ahmet C. Sabuncu[a], Janna Grubbs[b], Shizhi Qian[a], Tarek M. Abdel-Fattah[c], Michael W. Stacey [b],

Ali Beskok[a,1]

[a] Institute of Micro & Nanotechnology, Old Dominion University, Norfolk, VA 23529, USA

[b]Frank Reidy Research Center for Bioelectrics, Old Dominion University, Norfolk, VA 23529, USA

[c] Applied Research Center, Jefferson National Laboratory and Department of Molecular Biology and Chemistry, Christopher Newport University, Newport News, VA 23606, USA

Abstract

Nanoparticle research is often performed *in vitro* with little emphasis on the potential role of cell culture medium. In this study, gold nanoparticle interactions with cell culture medium and two cancer cell lines (human T-cell leukemia Jurkat and human pancreatic carcinoma PANC1) were investigated. Gold nanoparticles of 10, 25, 50, and 100 nm in diameter at fixed mass concentration were tested. Size distributions and zeta potentials of gold nanoparticles suspended in deionized (DI) water and Dulbecco's Modified Eagle's Media (DMEM) supplemented with fetal calf serum (FCS) were measured using dynamic light scattering (DLS) technique. In DI water, particle size distributions exhibited peaks around their nominal diameters. However, the gold nanoparticles suspended in DMEM supplemented with FCS formed complexes around 100 nm, regardless of their nominal sizes. The DLS and UV-vis spectroscopy results indicate gold nanoparticle agglomeration in DMEM that is not supplemented by FCS. The zeta potential results indicate that protein rich FCS increases the dispersion quality of gold nanoparticle

---

[1] Corresponding author: Tel.: +1 757 683 6818. Fax: +1 757 683 3200. E-mail address: abeskok@odu.edu.

1

suspensions through steric effects. Cellular uptake of 25 and 50 nm gold nanoparticles by Jurkat and PANC1 cell lines were investigated using inductively coupled plasma-mass spectroscopy. The intracellular gold level of PANC1 cells was higher than that of Jurkat cells, where 50 nm particles enter cells at faster rates than the 25 nm particles.

Introduction

Perhaps one of the earliest use of colloidal gold in medicine was to diagnose syphilis in the Middle Ages [1]. Through technological advancement in the late 20th and 21st centuries, unique optical, electronic, and chemical properties of gold nanoparticles were revealed. Several review papers report these properties and applications of gold nanoparticles in various fields [1-3]. The inert core, ease of functionalization, and surface plasmon oscillation of colloidal gold renders them excellent vehicles for bio-nano-analytic applications and targeted drug delivery. An application of gold nanoparticles in bio-nano-analytics used gold nanoparticles that produce optical response when microalbumin is present in urine [4]. One other study utilized anti-epidermal growth factor receptor conjugated gold nanorods for photothermal cancer therapy [5]. The biotechnology applications of gold nanoparticles require them to be suspended in biologically relevant buffers, including cell culture media. Upon contact with a physiological buffer, a new interface with unique characteristics develops at the gold surface [6]. For instance, the protein corona that forms on gold surfaces determines the colloidal stability and the cellular uptake of nanoparticles [2, 7, 8]. Successful engineering of biotechnology applications utilizing gold nanoparticles includes the characterization of their size, shape, agglomeration state, chemical composition, surface area, surface chemistry, and surface charge when gold nanoparticles are suspended in physiological media, and which is the objective of this study.

Colloidal properties of gold nanoparticles of different diameters (10, 25, 50, and 100 nm), such as aggregate size, morphology, and interfacial chemistry in physiological solutions were investigated. The gold nanoparticles were suspended in a commonly used cell culture media, namely Dulbecco Modified Eagle's Medium (DMEM) supplemented with protein-rich fetal calf serum (FCS). In order to test the particle properties in cell culture medium, a series of

experiments were performed with UV-vis absorbance spectroscopy, dynamic light scattering (DLS), electrophoretic light scattering (ELS), and transmission electron microscopy (TEM). The nature of colloidal interactions was explained by the DLVO (Derjaguin and Landau, Verwey and Overbeek) theory [9]. In addition, cellular uptake of gold nanoparticles by two human cell lines (Jurkat T-cell leukemia and human pancreatic carcinoma PANC1) was measured using inductively coupled plasma optical emission spectroscopy. Jurkat and PANC1 cells are structurally intrinsic, which allowed distinguishing nanoparticle interactions with adherent (PANC1) and suspension (Jurkat) cell lines. A toxicological investigation of gold nanoparticles was performed via the trypan blue exclusion technique on Jurkat and PANC1 cells.

Materials and Methods

Gold nanoparticles

The gold nanoparticles used in this study were purchased from Nanopartz Inc. (Loveland, USA). According to the manufacturer, the gold nanoparticles were capped with a carboxylic acid functionalized hydrocarbon agent (500 Da) and were used without any purification or treatment in this study. Four different sizes of gold nanoparticles (10, 25, 50, and 100 nm) were suspended in deionized (DI) water with <0.1% sodium hydroxide.

Preparation of gold suspensions

Dulbecco's Modified Eagle's Media (DMEM; ATCC, USA) cell culture medium was used in particle characterization studies. DMEM contains low amounts of inorganic salts, amino acids, vitamins, and glucose. The list of ingredients of DMEM as supplied from the manufacturer is given in Table S1. Unless otherwise stated, DMEM suspensions were supplemented with 10% (v/v) fetal calf serum, which contains bovine serum albumin protein plus many other proteins

essential for growth, and 1% of penicillin and streptomycin, yielding the same media constituents used for cell culturing. Small aliquots were taken from gold nanoparticle stock suspensions and pelleted by a benchtop centrifuge (Eppendorf Minispin, USA). Supernatants were removed from tubes and particles re-suspended in desired solutions. In some experiments DI water from an in-house system (Millipore, USA) was used. The test suspensions were mixed gently prior to experiments.

Particle characterization:

Gold suspensions were characterized by a particle analyzer and transmission electron microscopy. Both size and zeta potential measurements of gold suspensions were conducted using a particle analyzer (Delsa Nano, Beckman Coulter, Inc.) that utilizes DLS and ELS techniques. The light scattering experiments were conducted using 658 nm laser light. The DLS technique and the method of averaging the DLS data were described in detail in a previous publication [10]. All experiments were repeated at least 3 times. For long-term DLS studies the sample was kept at $37^{o}C$ between time points. The samples were measured 2 minutes after preparation. The details of the ELS measurement technique are given in the supporting information.

Henry's equation [11] was used to estimate the zeta potential from the electrophoretic mobility,

$$\mu = \frac{\zeta \varepsilon}{\eta} f(\kappa r)$$

(1)

where ζ is the zeta potential, $f(\kappa r)$ is the Henry's function, κ and r are the Debye length and particle radius, respectively. Henry's function reaches 1 for κr approaching 0, which is known as the Hückel-Onsager limit; it converges to 1.5 for κr approaching infinity, which is known as

5

the Helmholtz-Smoluchowski limit. In this study, values of κr for gold nanoparticles in different buffers were computed and the Henry's function evaluated using the following approximation developed by Ohshima [12]:

$$f(\kappa r) = \frac{2}{3}\left[1 + \frac{1}{2\left(1 + \left(2.5/\kappa r\left(1 + 2\exp(-\kappa r)\right)\right)\right)^3}\right]. \tag{2}$$

Henry's approach assumes that (1) the total electric field is the superposition of the external electric field and electric field arising from the charged surface; (2) polarization of the double layer is negligible; (3) Zeta potential is low ($e\zeta/k_bT \ll 1$); and (4) the particle is insulating. The last assumption might seem inapplicable for gold colloids; however, experimental observations suggest that they indeed behave as insulator colloids [13, 14]. As the electric field inside gold, which is a good conductor, is zero; the current should be carried on the surface. For gold colloids suspended in aqueous solutions, surface conductivity might be low due to adsorbed species, and therefore, colloidal gold behaves as insulators.

Gold nanoparticles were also observed by transmission electron microscopy. A test solution of 10 µl volume was placed on carbon coated 300 mesh copper grid (TEDPELLA Inc, Redding USA) and air dried for 24 hours. The grids were observed under high resolution transmission electron microscope (JEM-2100F, JEOL Ltd, Japan) operating at 200 kV; and Feret diameters of the nanoparticles were determined. Recorded images were processed using the ImageJ Software (v1.38x, NIH, USA) to extract the Feret diameter and circularity values. The Feret diameter is defined as the longest distance between any two points on the boundary of the particle.

UV-vis spectroscopy

UV-vis absorption spectra were collected with SHMADZU UV-2401 PC, UV-vis spectrophotometer.

Cell lines & cell culture

Toxicity and cellular uptake experiments were performed on the pancreatic cancer derived cell line PANC1, and the T-cell leukemia cell line, Jurkat (ATCC, Manassas, USA). PANC1 and Jurkat cells were grown in DMEM and Roswell Park Memorial Institute (RPMI; ATCC, USA) respectively. Both types of growth medium were supplemented with glutamine, penicillin, streptomycin, and 10% fetal bovine serum. Cells were grown in a humidified atmosphere with 5% CO_2 at 37°C.

Cell viability

Exponentially growing cells were adjusted to a concentration of 2×10^5 cells/ml and plated into triplicate wells. Gold nanoparticles of 25 nm and 50 nm in diameter were introduced to cells at a final concentration of 10 μg/ml. Control cells were exposed to the same volume of carrier medium without nanoparticles. Cells were grown for 24 and 48 hours. Cell viability was measured by trypan blue exclusion, which is a vital dye that stains dead cells blue, while leaving live cells clear. Cells were mixed with trypan blue, and the mixture was loaded onto a hemocytometer. The numbers of live (unstained) and dead (stained) cells were counted and cell viability determined as the number of live cells/total cell number ×100%. Experimental wells were normalized to unexposed controls.

Intracellular gold content measurements

PANC1 and Jurkat cells were used for intracellular gold content measurements where 2×10^5 cells were incubated at 37°C for 24 hours in the presence of 25 nm and 50 nm gold nanoparticles. The nanoparticle mass concentration was 10 μg/ml. Floating Jurkat cells were transferred directly to centrifuge tubes. Adherent PANC1 cells were removed from the surface of the well plates by TrypLE™ digestion (Invitrogen, Carlsbad, USA). Cells were fixed with 4%

paraformaldehyde in order to prevent the cells from losing nanoparticles during subsequent steps. Cells were washed 3 times with Hank's buffered salt solution (MediaTech, Manassas, VA, USA) to dispel extracellular gold. Finally, cells were digested in concentrated nitric acid, and analyzed for gold content. All samples were prepared in triplicates. All gold concentrations were measured utilizing inductively coupled plasma (ICP) optical emission spectroscopy using Varian 720-ES. All ICP standards were made from 100 mg/ml stock solution, and all ICP samples were analyzed at 208.207 nm with a read delay of 80 s and an integration time from 2 to 5 s.

Results and Discussion

Size and morphology of gold nanoparticles

Typical electron micrographs of gold nanoparticles are shown in Figure 1. Figure 1(a) depicts an individual gold particle, while Figure 1 (b) shows several nanoparticles with a different length scale. Dynamic light scattering was employed to measure the hydrodynamic diameter of nanoparticle suspensions. Figures 2 (a) and (b) depict, respectively, the intensity-based size distributions of 10 nm, 25 nm, 50 nm, and 100 nm particles suspended in DI water and DMEM. The peak values of the size distribution spectra from the data shown in Figure 2 and polydispersity (PI) indexes of the corresponding samples are listed in Table 1. Based on Table 1 and Figure 2, the mean size of the particles suspended in DMEM was higher than the mean of those in DI water. Particles tend to form larger complexes in DMEM. Interestingly, regardless of their nominal sizes, particles form complexes around 100 nm. The PI indexes of the particles suspended in DMEM were higher than those suspended in DI water, implying that gold nanoparticles suspended in DMEM have broader size distributions. UV-vis spectra of 10, 25, and 50 nm gold nanoparticles suspended in DI water and DMEM are given in the supporting

8

information (Figures S1). In DI water, absorbance gives a peak around 520 nm; whereas the peak is red-shifted to around 550 nm as the particles are suspended in DMEM. Figure 3 compares the UV-vis absorbance spectra of 10 nm gold nanoparticles suspended in DI water, DMEM, and DMEM without FCS. The peak around 520 nm disappears for the particles suspended in DMEM without FCS, suggesting aggregation in this medium. The DLS spectrum of pure DMEM (supporting information, Figure S2) shows no protein aggregation in DMEM.

In order to understand the effects of ionic strength and various elements in cell culture medium on dispersion state, gold nanoparticles of 10 nm in diameter were suspended in various buffers: namely DI water, DI water supplemented with FCS (10% v/v), DMEM, DMEM without FCS, 12 and 124 mM NaCl solutions. The electrical conductivities of DI water and DI water supplemented with FCS are 5.2×10^{-4} S/m and 0.15 S/m, respectively. The molarities of the NaCl solutions were adjusted to mimic DMEM and DI water supplemented with FCS. By preparing buffers in these ways, the effects of ionic strength and FCS proteins on the dispersion state were tested. Figure 4 shows intensity-based size distributions of particles suspended in the aforementioned solutions, except for the 12 mM NaCl suspension. The suspension dispersion quality is judged by its deviation from the nominal size. Accordingly, dispersion quality of the samples can be sorted as follows: DI > DI + FCS > DMEM > 124 mM NaCl > DMEM without FCS.

Electrophoretic mobility measurements were conducted for the gold nanoparticles suspended in the following solutions: DI, DI suspended with FCS, DMEM cell culture medium, DMEM without FCS, and NaCl suspensions of 12 and 124 mM. In order to accurately calculate the zeta potential, Henry's equation was utilized. Henry's function requires particle diameter and Debye length as input parameters; therefore, for each suspension mean value of strongest peak in the

DLS size distribution was considered as the particle size. For DMEM, only contributions from NaCl, KCl, and $NaHCO_3$ were considered during calculations since other salts are less than 2 mM and do not introduce significant errors on zeta potential calculation (Table S1). Conductivity, mean particle diameter, mobility, and zeta potential for the suspensions are summarized in Table 2. Zeta potentials of the gold nanoparticles can be sorted as the following with respect to the solutions they are suspended in (as absolute values): DI>12 mM NaCl >DI+FCS>124 mM NaCl>DMEM without FCS. The order of zeta potentials is in accordance with the size distributions shown in Figure 4, except for the suspensions with FCS. The DI suspension had the largest zeta potential and the best dispersion quality. The suspension with 124 mM NaCl yielded higher zeta potential (absolute) than DMEM without FCS that has the same ionic conductivity. The zeta potentials of 12 mM NaCl and DI with FCS are similar. Electrophoretic mobilities of gold nanoparticles suspended in NaCl solutions of varying molarity, 1:1 diluted, and pure DMEM are shown in Figure 5 (a).

The pH of NaCl solutions and DMEM were measured to be approximately 7.4. As the ionic strength increases, the mobility for both suspensions decreased. The mobility of the particles suspended in DMEM solutions were lower than those suspended in NaCl solutions. The corresponding surface charge densities of the gold particles were calculated by theory given in a study by Ohshima [15]. The electric charge in the Stern layer was neglected when calculating the surface charge. In other words, the surface of the particles was assumed to coincide with the hydrodynamic slip plane.   The surface charge densities of the particles suspended in NaCl solutions and DMEM are shown in figure 5 (b). The surface charge densities for both suspension types increased as ionic strength increases, and the surface charge density of particles suspended in DMEM was lower than those suspended in NaCl solutions.

10

DLVO theory of colloidal stability can be utilized to explain the nature of colloidal interactions. Basically, the interaction between two colloids is dominated by two main forces: electrostatic repulsion and van der Waals attraction. The repulsive force stems from the electrostatic interaction between the similarly charged double layers. According to the London theory, the attractive van der Waals force results from the interaction between a temporary dipole on one material and an induced dipole on the other material. This molecular force can be pair-wise summed to account for the whole material. Hence, the total interaction potential between two materials is given as the following [9]:

$$V_T = V_R^{\psi} + V_A = 2\pi\,\varepsilon\,a\,\psi_0^2\,\ln\left[1 + \exp(-\kappa H)\right] - \frac{a\,A_{gwg}}{12H}, \tag{3}$$

where V_R^{ψ} is the repulsive potential at fixed surface potential, V_A is the attractive potential, a is the particle radius, ψ_0 is the surface potential, κ is the reciprocal of Debye length, H is the separation distance between the particles, and A_{gwg} is the Hamaker constant for gold-water-gold interface. In addition to the electrostatic repulsion and attractive van der Waals interactions, several forces play a role in particle-particle interaction. The following can affect the colloidal stability: hydrodynamic, solvent, steric, and polymer bridging interactions [6].

The collision rate between the single spherical particles can be written as the following,

$$R = \frac{8k_bT}{3\mu} \cdot \frac{1}{2a\int_{2a}^{\infty}\frac{1}{r^2}\exp(V_T/k_bT)\,dr}\,n_0^2 \tag{4}$$

where k_b is the Boltzmann constant, T is the temperature of the system, and μ is the viscosity. It can be inferred from the above equation that the collision rate between the colloids scales with the square power of the particle concentration. According to equation (4), the collision rate

decreases as the interaction potential between the particles increases. An increase in the interaction potential requires an increase in the repulsive part of the potential, which acts as a barrier between the particles. Moreover, a temperature increase in the system can affect the stability by increasing the collision rate. The above analysis of colloidal stability supports the results presented here. In low conductivity buffers such as DI water, the double layer is thicker, and the repulsive force field is long range. As particles are suspended in a physiological medium, the double layer thickness decreases, and therefore, the repulsive potential in equation (3) becomes less effective in the long range to prevent agglomeration. Therefore, agglomeration is prominent in physiological solutions without FCS, which is obvious from Figure 4. Larger sized particles become pronounced in the intensity-based size spectra when the nanoparticle mass concentration is increased by a factor of 5 (Figure S4). The collision rate increased as the nanoparticle mass concentration is increased.

Zeta potential is an important parameter in the repulsive electrostatic force between the particles (equation 3). The repulsive force scales with the square of the surface potential. In addition, the higher the zeta potential the longer the range of repulsive force. Therefore, suspension stability is enhanced by increased zeta potential. Gold nanoparticles in DI water have the highest zeta potential among other suspensions listed in Table 2. Accordingly, it has the best dispersion quality, as shown in Figure 4. Zeta potential of the colloids gradually decreased, as the ionic strength increased from that of DI water to physiological ionic strength (~130 mM). This decrease is obvious from both Table 2 and Figure 5 (a). The decrease in zeta potential also causes a decrease in dispersion quality. Interestingly, the zeta potential of FCS suspension is a little lower than that of the NaCl solution with the same ionic conductivity; however, FCS suspension yields better dispersion states than the NaCl suspension (Table 2). The same is true

12

for DMEM suspensions with and without FCS where there is a substantial difference between the dispersion qualities of DMEM suspensions. This suggests a specific interaction between FCS constituents and gold nanoparticles, which is further supported by red-shift in the UV-vis spectra of nanoparticles suspended in DI water and DMEM (Figures S1 (a) and (b)). Several serum proteins such as albumin, immunoglobulin, and fibrinogen were found to bind on nanoparticles [6]. Absorption of proteins on gold nanoparticles enhances the colloidal stability through steric mechanisms. Adsorbed proteins on the particle surface act like spring structures that exert a repulsive force inhibiting contact between particles, and thereby increasing the colloidal stability. The steric hindrance force can be represented by an extra potential term in equation 3. According to Figure 2 (b), as different sized gold nanoparticles were suspended in DMEM at fixed mass concentration, they formed similar sized structures. Remarkably, the increase in the mean size of 10 nm gold nanoparticles as they were suspended in DMEM was substantial. Accordingly, the protein corona on 10 nm gold nanoparticles was the largest. The overall size is influenced by the degree of the surface curvature. This suggests dependence of protein adsorbance on the nanoparticle size. Moreover, evolution of the normalized peak value of the size distribution over 48 hour period is given in supporting information (Figure S3). The size reached a plateau after 24 hours of incubation at 37°C.

There are two main hypotheses for the explanation of the interaction between proteins and gold nanoparticles [16]. The electrostatic binding hypothesis states that the electrostatic interaction between charged surface residues of the protein (for instance from protonation of the charge groups) and charged surface groups (for instance negatively charged ligands) are responsible for the binding. The other hypothesis states that the stabilizing monolayer on the surface is replaced by the proteins during adsorption. Gold nanoparticles used in this study were produced with a

hydrocarbon-capping agent (500 Da) that was carboxylic acid functionalized. This monolayer is responsible for the net negative charge and the surface reactivity. However, according to the gold nanoparticle's manufacturer, the nanoparticle's capping agent is adsorbed onto the nanoparticle surface by weak van der Waals forces. Following this fact, the weak bonds between surface and capping agent are easily replaced by protein-gold bonds. Different binding mechanisms were observed in previous studies: The most abundant serum protein albumin was found to bind on citrate stabilized gold nanoparticles by the fist way described above, rather than exchanging the stabilizing monolayer [16]. The same way of binding of albumin, myoglobin, and cytochrome c, was observed on mercaotoundecanoic acid stabilized gold nanoparticles [17].

The increase in the surface charge density with ionic strength, shown in Figure 5 (b), can be best described by preferential solubility of the ions in the interfacial region [18]. In addition to the preferential solubility of ions, the hydrated ions might lose their hydration shells and bind to the gold surface. However, this process is thermodynamically unfavorable. The suspension of gold nanoparticles in DMEM yielded lower surface charge density, which might be due to the following reasons: (1) adsorption of positively charged or uncharged aminoacids (such as L-Glutamine that is abundant in blood serum) and (2) differential solubility of ions of the cell culture medium in the interfacial region. The adsorbed aminoacids are larger than hydrated ions. Therefore, following the above-mentioned facts, the effective area of net negative nanoparticle charge decreased in DMEM.

There is a correlation between the morphology of the agglomerates and colloidal stability [19]. Depending on the ionic strength, the agglomerates might be formed in one, two, and three-dimensional fashions. At low ionic strengths where the repulsive forces between the particles are effective, the trajectory of one particle is along the axis of symmetry of a doublet. This in turn

generates a triplet, and particles form linear aggregates as a result. Two-dimensional agglomerates form at moderate electrolyte concentrations. In two-dimensional formations, particles tend to adhere to sides of the particle groups, and thereby planar particle groups are formed. Three-dimensional agglomerates form as a result of fast coagulation, for example, when the potential barrier between particles disappears at high electrolyte concentrations. Examination of the TEM micrographs of particles provides information on the degree of coagulation. Such 3-D agglomerates are observed for gold nanoparticles suspended in DMEM without FCS, and are presented in Figures 1 (b) and S5.

Intracellular gold content measurements

Intracellular gold contents of Jurkat and PANC1 cells were analyzed by ICP optical emission spectroscopy after 24 hours of incubation with gold nanoparticles in RPMI and DMEM, respectively. Cells were incubated with 25 and 50 nm gold nanoparticles. Mass concentration of gold was kept constant in the experiments (10 µg/ml). Accordingly, the number concentration of samples with 25 nm gold was higher than the samples with 50 nm gold. The gold mass internalized by each cell, shown in Figure 6, was calculated in picograms from the gold concentration that was measured by ICP optical emission spectroscopy. The amount of gold entered PANC1 cells was more than that of Jurkat cells, and 50 nm particles were found at higher levels than 25 nm particles.

The cell membrane permits the diffusion of small nonpolar molecules and uncharged polar molecules through its membrane. For example water, O_2, CO_2, ethanol, and glucose can pass the cell membrane by diffusion. However, nanoparticles are incapable of crossing the cell membrane by diffusion due to their large size. Cellular uptake of nanoparticles is determined by their protein corona. It has been previously reported that receptor specific binding of gold

15

nanoparticles on the cell surface is followed by membrane wrapping and endocytotic uptake of nanoparticles [2, 20]. Assuming non-specific adsorption of serum proteins by gold nanoparticles, multiple serum proteins attached to the nanoparticles will allow entry through multiple receptor sites (for example receptor-mediated phagocytosis). Alternatively, a greater array of divergent receptors may be present on the surface of PANC1 cells, allowing for greater uptake of nanoparticles through multiple receptor sites in this cell type. Chitrani [20, 21] reported 50 nm as the optimum diameter for uptake of transferin-coated gold nanoparticles. The results in figure 6 indicate higher uptake of 50 nm gold nanoparticles at the same mass concentrations. Interestingly, according to the results in Figure 2 (b) and Table 2, 25 and 50 nm gold particles form similar sized complexes with the former having a broader size distribution. However, the type of proteins that surround particles might differ between 25 nm and 50 nm particles, depending on the degree of surface curvature [7]. Accordingly, the results in Figure 6 indicate the importance of cell receptor-protein interactions on cellular uptake of nanoparticles rather than dependency of uptake on the nominal size.

Cellular toxicity

Nanoparticles appeared to be non-toxic to Jurkat and PANC1 cells. Jurkat cells grown in the presence of 25 nm and 50 nm nanoparticles at 10 µg/ml concentration showed viability of 102% and 93%, respectively at 24 hours normalized with unexposed controls (100%); and 99% and 100%, respectively at 48 hours. The PANC1 cells showed viability of 107% and 124% normalized with the unexposed controls when grown for 24 hours in the presence of 25 nm and 50 nm nanoparticles, and 91% and 83%, respectively at 48 hours.

Conclusions

16

In this study, the behavior of gold nanoparticles in cell culture media was investigated. Four different sizes of gold nanoparticles at the same mass concentration were tested in culture media in the presence and absence of fetal calf serum. Dynamic light scattering, electrophoretic light scattering, UV-vis spectroscopy, and transmission electron microscopy were employed to gain insights on the dispersion state of nanoparticles. Nanoparticles formed similar sized particle complexes when suspended in DMEM. The results suggest agglomeration of nanoparticles in DMEM without FCS. The size of the agglomerates was found to increase with increasing nanoparticle concentration. The nanoparticles were found to be stable over long time periods (48 hours). Zeta potential measurements were carried out by the electrophoretic light scattering technique to gain insights into the interfacial chemistry in culture media. Results showed that fetal calf serum increased the dispersion quality of nanoparticles without increasing the zeta potential, likely due to steric forces. The intracellular gold levels of Jurkat and PANC1 cells were analyzed by inductively coupled plasma optical emission spectroscopy and showed more gold particles in PANC1 cells compared to Jurkat cells. At the same mass concentration, 50 nm diameter gold nanoparticles entered cells more readily than 25 nm particles. According to the DLS results, 25 and 50 nm particles formed complexes of similar sizes in DMEM. Thereby, the type of protein corona around the particle appears to play a crucial role in nanoparticle uptake. At the same mass concentration, gold nanoparticles were found to be non-toxic to the cells. These observations are critical while designing cargo vehicles for drug delivery or for delivery of nanoparticles for other therapeutic purposes. In addition, the relative contributions of different uptake mechanisms, such as the receptor mediated phagocytosis and direct penetration, in specific cell types could be another avenue of future research. Investigation of uptake mechanisms of different cell lines is clearly important future work.

Table 1. Locations of the peaks in the size spectra of gold nanoparticles from the data presented in figure 1. All units are in nanometers. In parentheses are the PI indexes.

Nominal Dia.	DI Water	DMEM
10	24(0.05)	108(0.29)
25	41(0.24)	95(0.30)
50	65(0.24)	88(0.26)
100	97(0.17)	110(0.17)

Table 2. Zeta potentials of gold nanoparticles suspended in DI water, DI water with FCS (10% v/v, 0.15 S/m), 12 and 124 mM NaCl solutions, DMEM cell culture medium, and DMEM cell culture medium supplemented with FCS (10% v/v). The data is presented as mean and standard deviation in parentheses.

	Conductivity $[\mu S / cm]$	Mean Dia. $[nm]$	Henry's function $f(\kappa r)$	Mobility $[\mu m \cdot cm / V s]$	Zeta potential $[mV]$
DI Water	5	18	0.6682	-3.27(0.32)	-71.04(6.93)
DI + FCS	1510	85	0.8799	-1.78(0.8)	-29.34(13.16)
12 mM NaCl	1510	180	0.9344	-2.1(0.37)	-32.68(5.73)
DMEM	14400	190	0.9788	-1.49(0.36)	-22.04(5.32)
124 mM NaCl	14400	250	0.9833	-1.36(0.09)	-20.15(1.32)
DMEM wo FCS	14400	400	0.9896	-1.07(0.53)	-15.75(7.75)
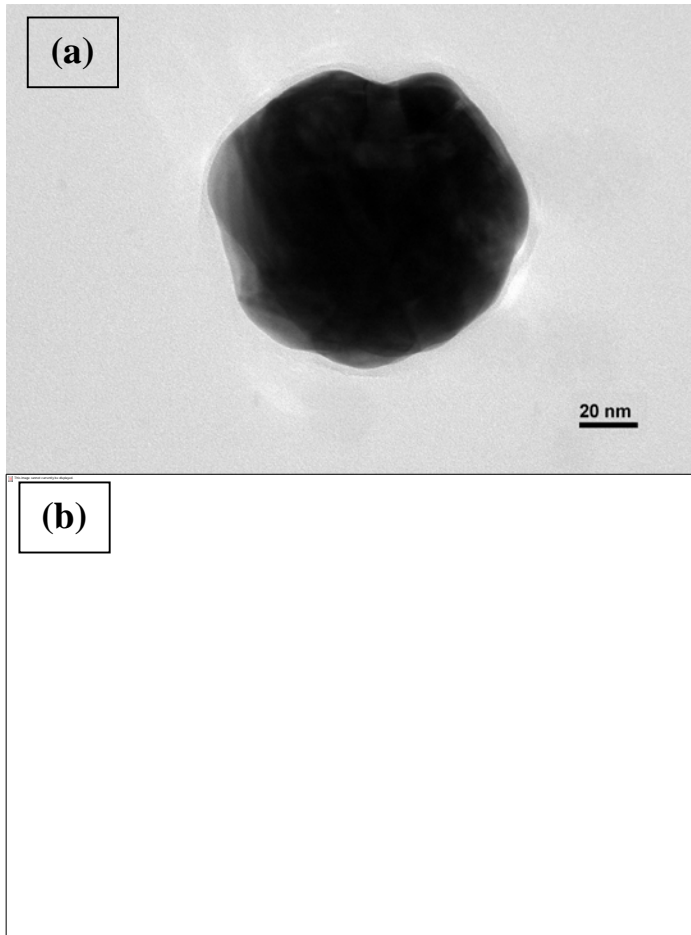
Fig. 1. Transmission electron microscopy images of gold nanoparticles of 100 nm diameter in DMEM (a), of 10 nm diameter in DMEM without FCS (b).
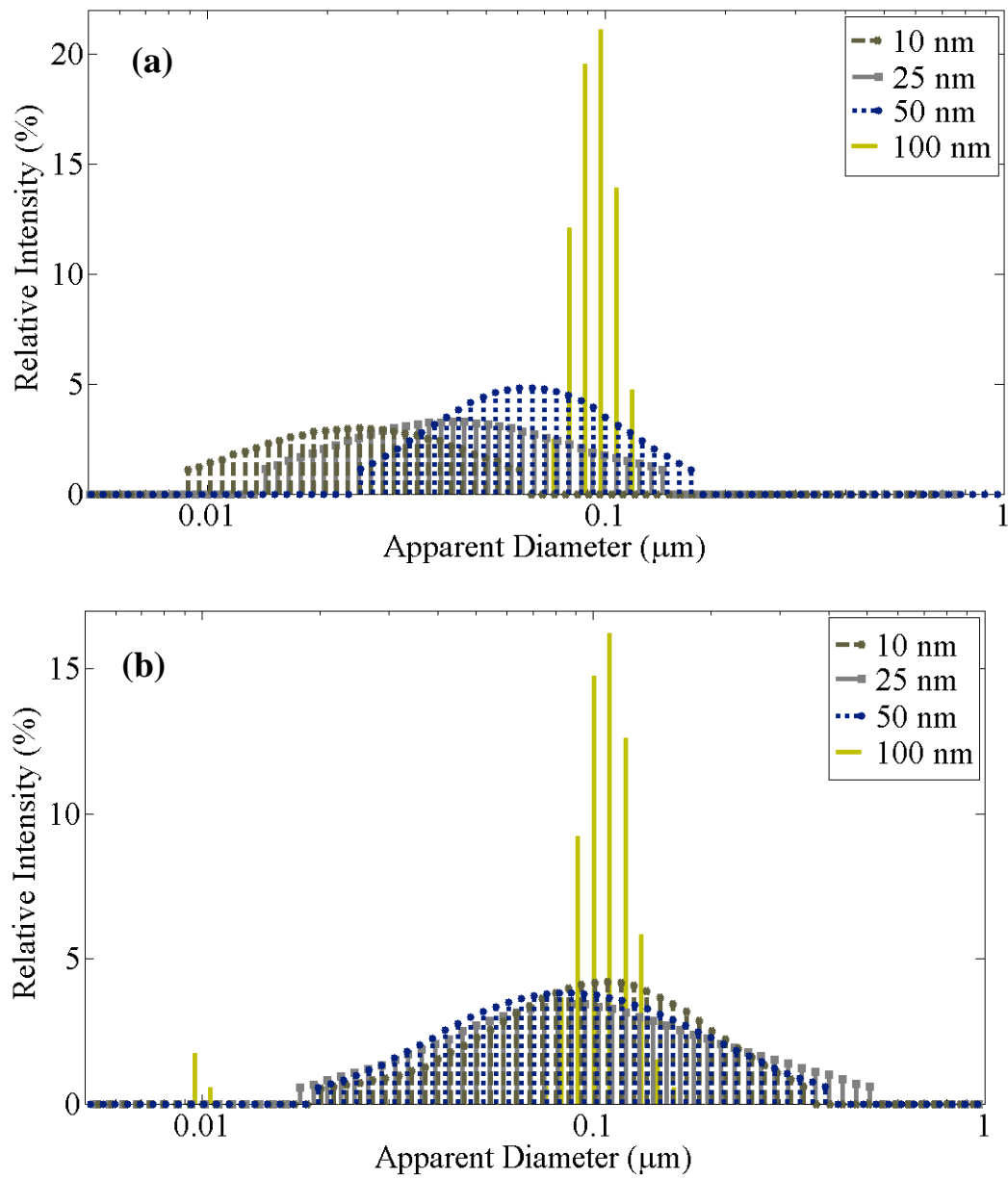
Fig. 2. Differential scattered light intensities from gold nanoparticles of 5 µg/ml concentration suspended in DI water (a), DMEM (b). Measurements were conducted at 37°C
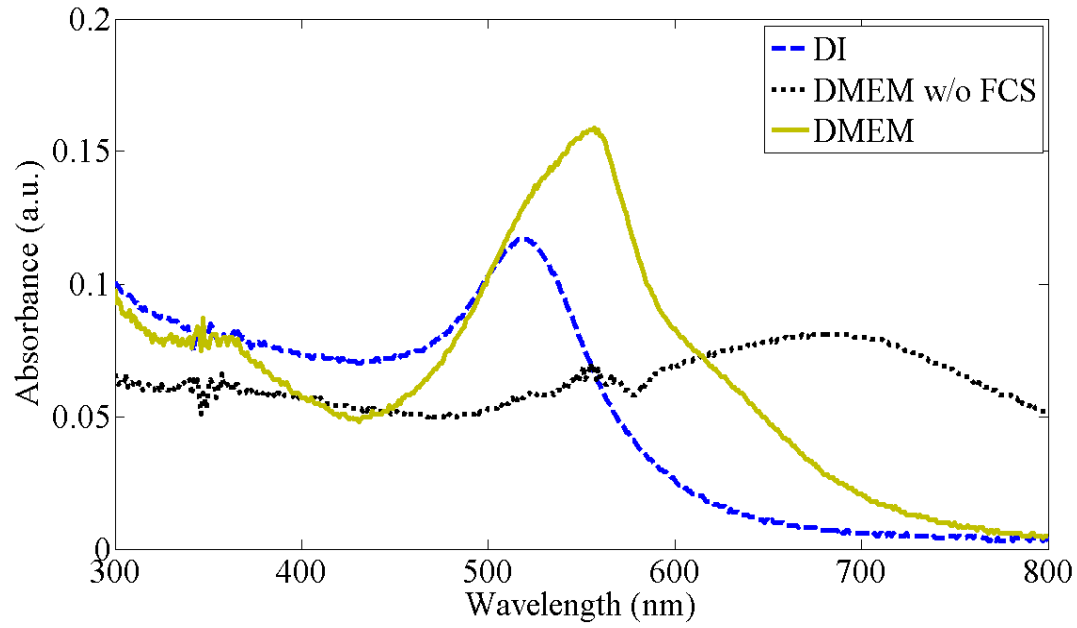
Fig. 3. UV-vis spectra of gold nanoparticles of 10 μg/ml concentration suspended in DI water (dashed line), DMEM (continuous line), and DMEM without FCS (dotted line).

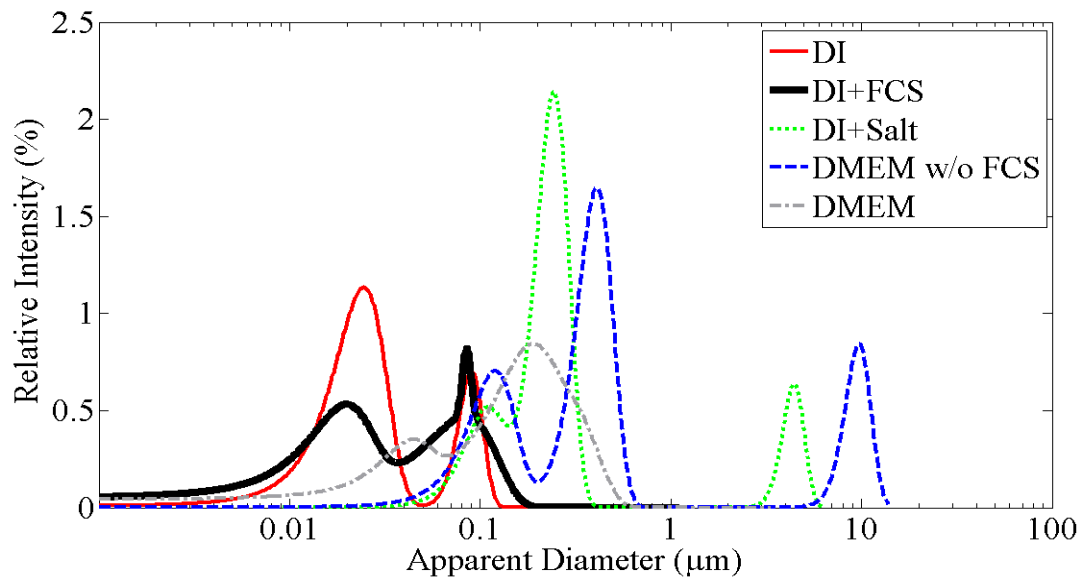Fig. 4. Differential scattered light intensities from 10 nm gold nanoparticles suspended in different buffers: DI water, DI water with FCS (10% v/v, 0.15 S/m), 124 mM NaCl solution (1.44 S/m), DMEM cell culture medium, DMEM without FCS.
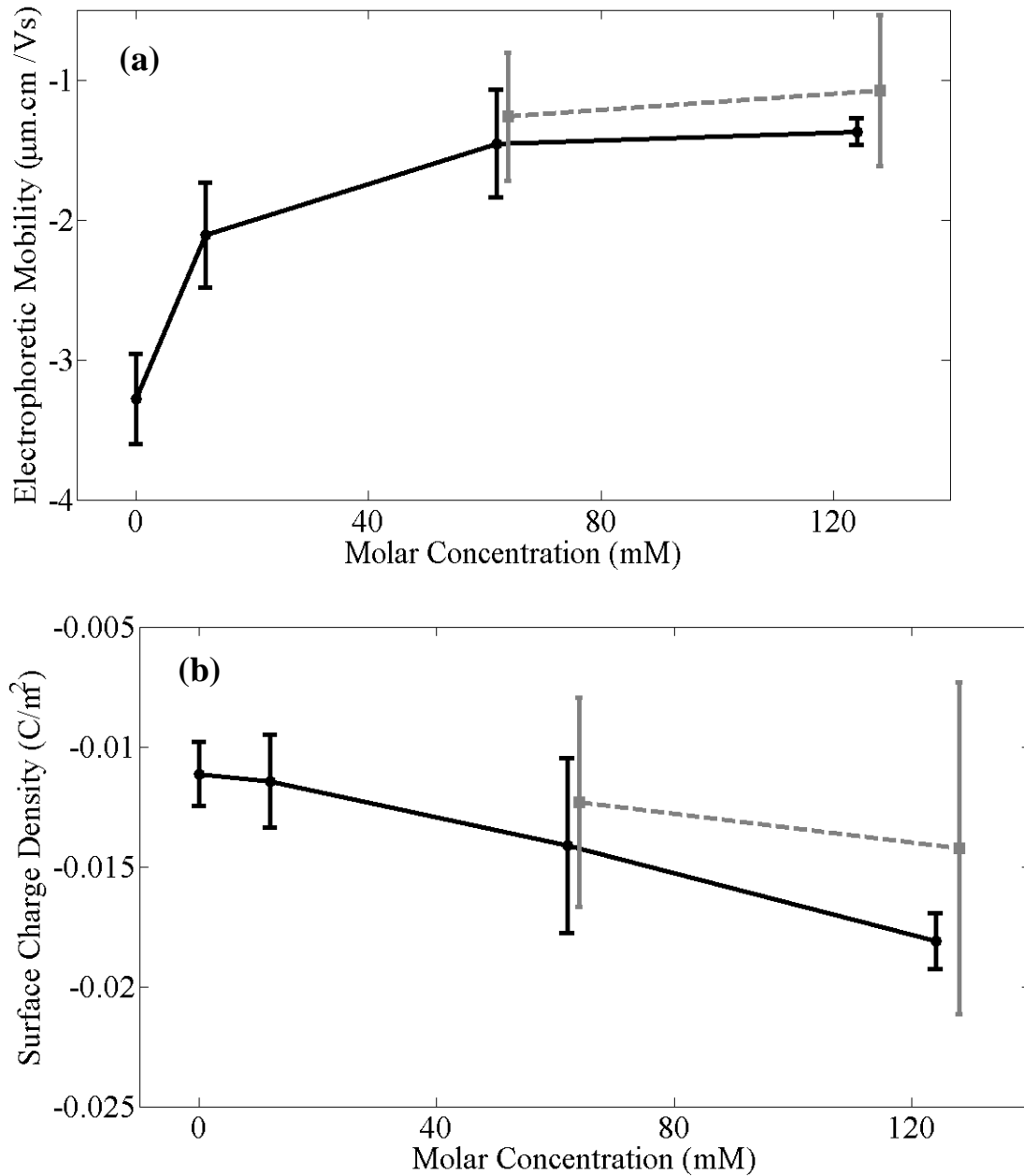
Fig. 5. Electrophoretic mobility (a) and surface charge density (b) of 10 nm gold nanoparticles suspended in NaCl solutions (continuous line) and in DMEM (dashed line). Particle concentration is 5 µg/ml.
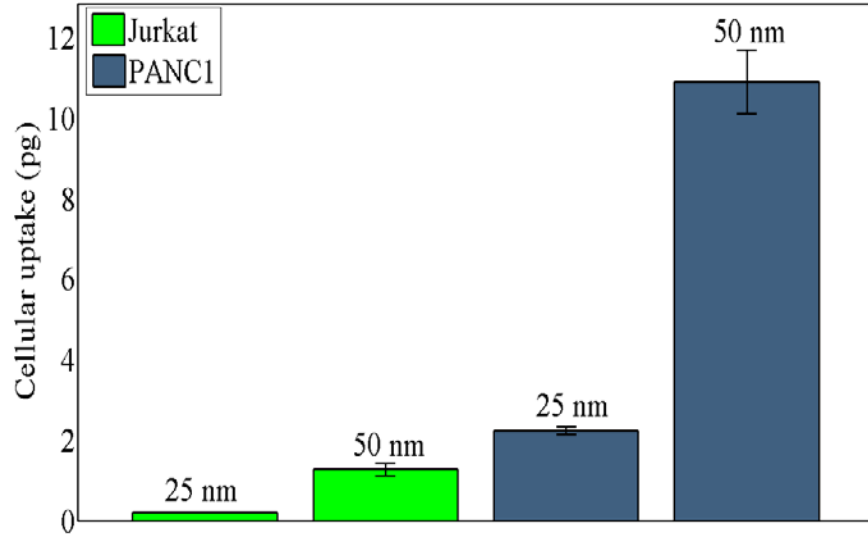
Fig. 6. Nanoparticle mass internalized by each cell. Jurkat and PANC1 cells were incubated with 25 nm and 50 nm gold nanoparticles for 24 hours.

References:

[1] M.-C. Daniel and D. Astruc, Gold Nanoparticles: Assembly, Supramolecular Chemistry, Quantum-Size-Related Properties, and Applications toward Biology, Catalysis, and Nanotechnology, Chemical Reviews, 104 (2004) 293-346.

[2] R. Lévy, U. Shaheen, Y. Cesbron and V. Sée, Gold nanoparticles delivery in mammalian live cells: a critical review, Nano Reviews, 1 (2010).

[3] S. Eustis and M.A. El-Sayed, Why gold nanoparticles are more precious than pretty gold: Noble metal surface plasmon resonance and its enhancement of the radiative and nonradiative properties of nanocrystals of different shapes, Chemical Society Reviews, 35 (2006) 209-217.

[4] V. Wiwanitkit, A. Sereemaspun and R. Rojanathanes, Gold Nanoparticle as an Alternative Tool for Urine Microalbumin Test: The First World Report, Renal Failure, 29 (2007) 1047-1048.

[5] X. Huang, I.H. El-Sayed, W. Qian and M.A. El-Sayed, Cancer Cell Imaging and Photothermal Therapy in the Near-Infrared Region by Using Gold Nanorods, Journal of the American Chemical Society, 128 (2006) 2115-2120.

[6] A.E. Nel, L. Madler, D. Velegol, T. Xia, E.M.V. Hoek, P. Somasundaran, F. Klaessig, V. Castranova and M. Thompson, Understanding biophysicochemical interactions at the nano-bio interface, Nat Mater, 8 (2009) 543-557.

[7] E. Casals, T. Pfaller, A. Duschl, G.J. Oostingh and V. Puntes, Time evolution of the nanoparticle protein corona, ACS nano, 4 (2010) 3623-3632.

[8] G. Maiorano, S. Sabella, B. Sorce, V. Brunetti, M.A. Malvindi, R. Cingolani and P.P. Pompa, Effects of Cell Culture Media on the Dynamic Formation of Protein– Nanoparticle Complexes and Influence on the Cellular Response, ACS nano, (2010).

[9] R.J. Hunter, Foundations of Colloid Science, Second ed., Oxford University Press, Oxford, 2001.

[10] A.C. Sabuncu, B.S. Kalluri, S. Qian, M.W. Stacey and A. Beskok, Dispersion state and toxicity of mwCNTs in cell culture medium with different T80 concentrations, Colloids and Surfaces B: Biointerfaces, 78 (2010) 36-43.

[11] D.C. Henry, The Cataphoresis of Suspended Particles. Part I. The Equation of Cataphoresis, Proceedings of the Royal Society of London. Series A, 133 (1931) 106-129.

[12] H. Ohshima, A Simple Expression for Henry's Function for the Retardation Effect in Electrophoresis of Spherical Colloidal Particles, Journal of Colloid and Interface Science, 168 (1994) 269-271.

[13] S.M. Agnihotri, H. Ohshima, H. Terada, K. Tomoda and K. Makino, Electrophoretic Mobility of Colloidal Gold Particles in Electrolyte Solutions, Langmuir, 25 (2009) 4804-4807.

[14] K. Makino and H. Ohshima, Electrophoretic Mobility of a Colloidal Particle with Constant Surface Charge Density, Langmuir, 26 (2010) 18016-18019.

[15] H. Ohshima, Surface Charge Density/Surface Potential Relationship for a Spherical Colloidal Particle in a Solution of General Electrolytes, Journal of Colloid and Interface Science, 171 (1995) 525-527.

[16] S.H. Brewer, W.R. Glomm, M.C. Johnson, M.K. Knag and S. Franzen, Probing BSA Binding to Citrate-Coated Gold Nanoparticles and Surfaces, Langmuir, 21 (2005) 9303-9307.

[17] E.D. Kaufman, J. Belyea, M.C. Johnson, Z.M. Nicholson, J.L. Ricks, P.K. Shah, M. Bayless, T. Pettersson, Z. Feldotö, E. Blomberg, P. Claesson and S. Franzen, Probing Protein Adsorption onto Mercaptoundecanoic Acid Stabilized Gold Nanoparticles and Surfaces by Quartz Crystal Microbalance and ζ-Potential Measurements, Langmuir, 23 (2007) 6053-6062.

[18] D.E. Dunstan and D.A. Saville, Electrophoretic mobility of colloidal alkane particles in electrolyte solutions, Journal of the Chemical Society, Faraday Transactions, 88 (1992) 2031-2033.

[19] B.V. Enüstün and J. Turkevich, Coagulation of Colloidal Gold, Journal of the American Chemical Society, 85 (1963) 3317-3328.

[20] B.D. Chithrani and W.C.W. Chan, Elucidating the Mechanism of Cellular Uptake and Removal of Protein-Coated Gold Nanoparticles of Different Sizes and Shapes, Nano Letters, 7 (2007) 1542-1550.

[21] B.D. Chithrani, A.A. Ghazani and W.C.W. Chan, Determining the Size and Shape Dependence of Gold Nanoparticle Uptake into Mammalian Cells, Nano Letters, 6 (2006) 662-668.